iScience

Article

Identification of an immediate-early gene-activated fibroblast state in frozen shoulder capsular fibrosis

Graphical abstract

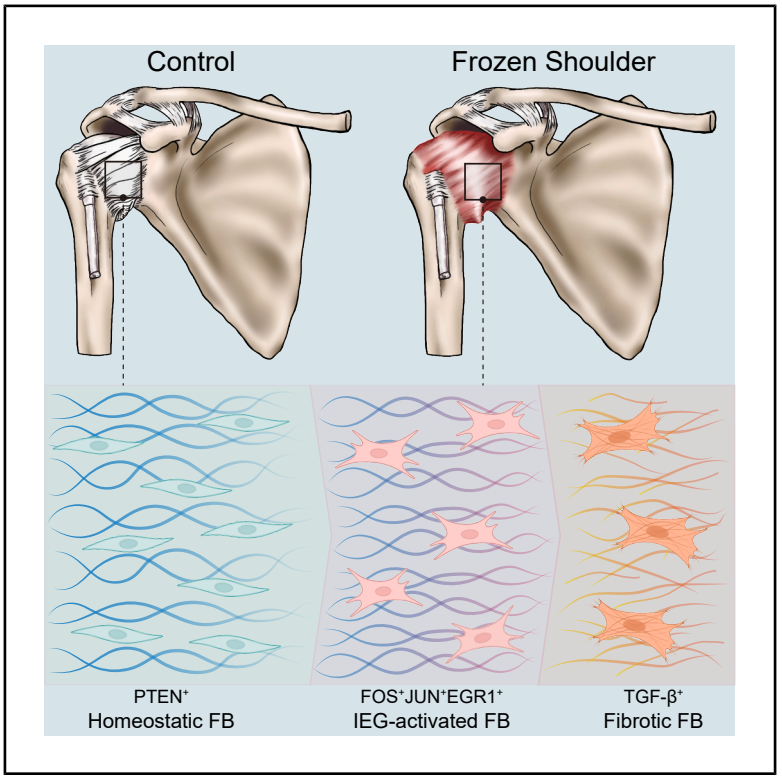

Authors

Zun Ren, Jie Lian, Renyuan Wang, ..., Haodong Lin, Dongsheng Jiang, Chunxi Yang

Correspondence

72400019193@shsmu.edu.cn (H.L.), dongsheng.jiang@sjtu.edu.cn (D.J.), chunxi_yang@163.com (C.Y.)

In brief

Health sciences; Medicine; Medical specialty; Orthopedics

Highlights

- Three fibroblast states in the shoulder capsule: homeostatic, IEG-activated, and pro-fibrotic
- A $FOS^+JUN^+EGR1^+$ fibroblast subset emerges in frozen shoulder
- The IEG-activated state is associated with capsular fibrotic remodeling
- Fibroblast state plasticity underlies frozen shoulder pathogenesis

Ren et al., 2026, iScience *29*, 116183
June 19, 2026
https://doi.org/10.1016/j.isci.2026.116183

CellPress

iScience

CellPress
OPEN ACCESS

Article

Identification of an immediate-early gene-activated fibroblast state in frozen shoulder capsular fibrosis

Zun Ren,[1,2,7] Jie Lian,[3,4,7] Renyuan Wang,[1,2] Wei Niu,[1,5] Xingyue Zhou,[1] Yilin Huo,[1,2] Haodong Lin,[2,*] Dongsheng Jiang,[1,2,*] and Chunxi Yang[3,6,8,*]

[1]Precision Research Center for Refractory Diseases, Shanghai General Hospital, Shanghai Jiao Tong University School of Medicine, Shanghai 201620, China
[2]Trauma Center, Shanghai General Hospital, Shanghai Jiao Tong University School of Medicine, Shanghai 201620, China
[3]Department of Orthopeadics, Shanghai General Hospital, Shanghai Jiao Tong University School of Medicine, Shanghai 201620, China
[4]Affiliated Hospital of Integrated Traditional Chinese and Western Medicine, Nanjing University of Chinese Medicine, Nanjing 210000, China
[5]School of Chemistry and Chemical Engineering, Shanghai University of Engineering Science, Shanghai 201620, China
[6]Department of Orthopedics, Renji Hospital, Shanghai Jiaotong University School of Medicine, Shanghai 200001, China
[7]These authors contributed equally
[8]Lead contact
*Correspondence: 72400019193@shsmu.edu.cn (H.L.), dongsheng.jiang@sjtu.edu.cn (D.J.), chunxi_yang@163.com (C.Y.)
https://doi.org/10.1016/j.isci.2026.116183

SUMMARY

Frozen shoulder (adhesive capsulitis) is characterized by progressive fibrotic remodeling of the shoulder joint capsule. To investigate the cellular programs underlying the fibrotic process, we integrate spatial transcriptomics, pseudotime inference, and *in situ* validation to comprehensively resolve fibroblast heterogeneity in human shoulder joint capsules. We identify three transcriptionally and spatially distinct fibroblast states: homeostatic, immediate-early gene (IEG)-activated, and pro-fibrotic. Notably, frozen shoulder exhibits a profound loss of homeostatic fibroblasts and a striking expansion of a $FOS^{+}JUN^{+}EGR1^{+}$ IEG-activated fibroblast subset that is rare in normal capsules. Trajectory analysis positions these cells as a stress-responsive transitional state linking homeostasis to fibrosis. Spatial mapping and immunostaining confirm the widespread emergence of IEG-activated fibroblasts in diseased capsules. Together, our findings identify an IEG-activated fibroblast state associated with fibrotic remodeling in frozen shoulder and highlight fibroblast state plasticity as a key contributor to disease pathogenesis.

INTRODUCTION

Frozen shoulder, also known as adhesive capsulitis (AC), is a common and disabling disorder in which progressive capsular fibrosis leads to chronic pain and severe restriction of shoulder motion. It most frequently affects individuals between 50 and 60 years of age, with an estimated prevalence of 2%–5% in the general population and a slightly higher incidence in women than in men.[1–3] AC is associated with multiple systemic and metabolic risk factors, including diabetes mellitus, thyroid dysfunction, hyperlipidemia, autoimmune diseases, cerebrovascular disease, smoking, and obesity.[4–11] Although traditionally regarded as a self-limiting condition that resolves within 1–2 years, accumulating evidence indicates that 20%–50% of patients experience persistent pain, stiffness, and functional impairment well beyond this time frame, substantially compromising quality of life.[12–14] Despite the availability of diverse therapeutic options, such as physiotherapy, manipulation under anesthesia, arthroscopic capsular release, hydrodilatation, and extracorporeal shockwave therapy, clinical outcomes remain variable, and complete symptom resolution is often not achieved.[15–21] These limitations underscore an incomplete understanding of AC pathogenesis.

At the tissue level, AC is defined by pathological remodeling of the glenohumeral joint capsule. In healthy shoulders, the joint capsule is thin, compliant, and elastic, providing stability while permitting a wide range of motion. In contrast, AC is characterized by capsular thickening and fibrosis involving both the fibrous and synovial layers, accompanied by chronic inflammation, neovascularization, and neoinnervation.[22–25] These structural alterations directly restrict joint mobility and contribute to pain. However, the cellular and molecular mechanisms driving this aberrant capsular remodeling remain incompletely defined, limiting the development of mechanism-based therapies.

Previous studies investigating AC pathogenesis have primarily focused on inflammatory and immune-mediated processes. Chronic, unresolved inflammation is a hallmark of AC, with infiltration of macrophages, mast cells, T cells, and B cells documented in affected joint capsules.[25,26] Pro-inflammatory cytokines such as IL-1β, IL-6, and TNF-α promote synovial inflammation, while skewing of macrophage polarization toward

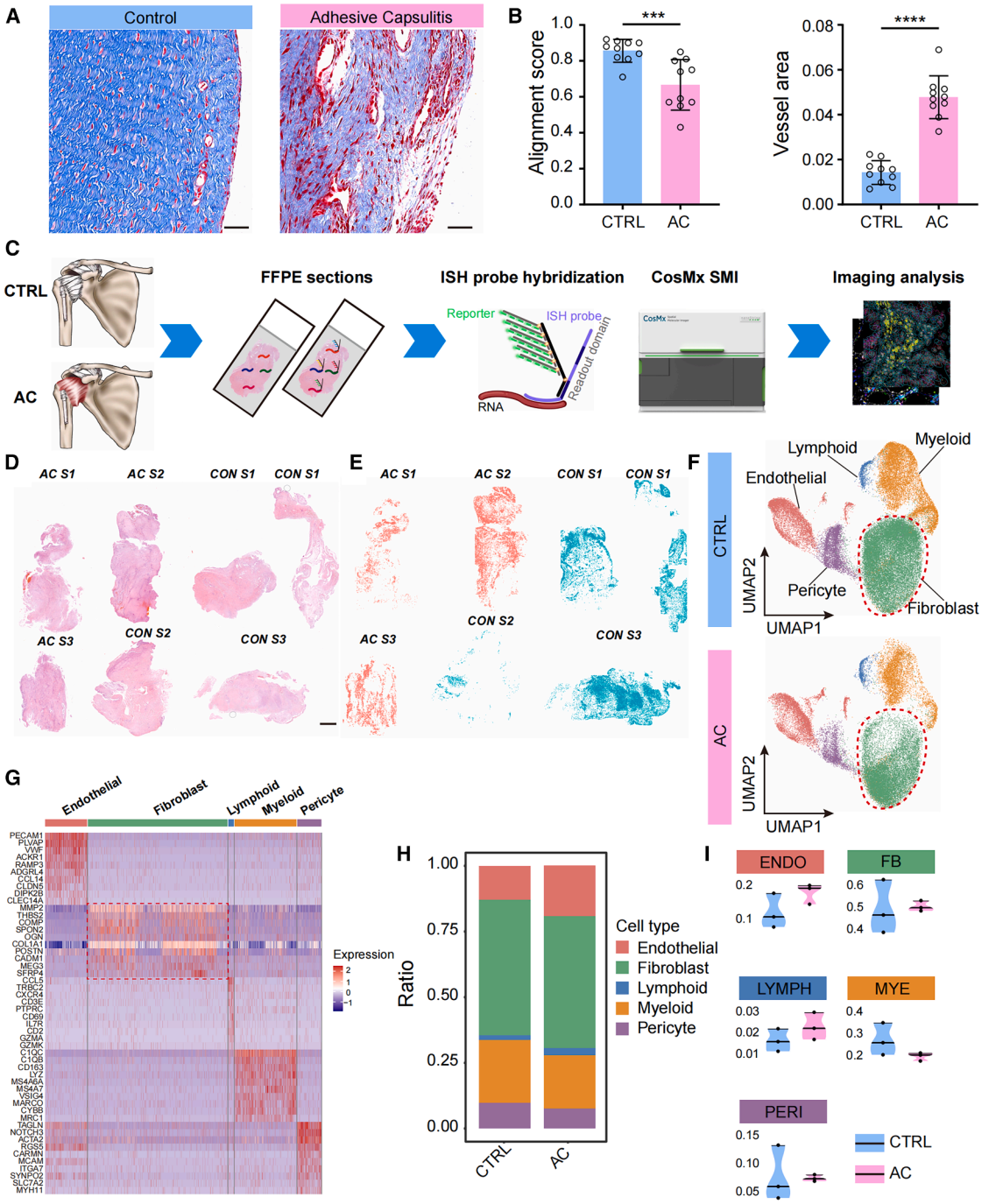

Figure 1. Spatial transcriptomics reveals a shift in fibroblast states in frozen shoulder

(A) Representative Masson's trichrome-stained sections of shoulder joint capsule tissues from control and adhesive capsulitis (AC) samples. Scale bars, 50 μm.

(B) Quantification of fiber alignment score and vessel area fraction derived from Masson's trichrome staining in control and AC tissues (n = 10).

(C) Schematic overview of the CosMx SMI spatial transcriptomics workflow. FFPE, formalin-fixed paraffin-embedded; ISH, *in situ* hybridization; SMI, Spatial Molecular Imager.

(D) Representative H&E-stained sections of samples subjected to spatial transcriptomic profiling. Scale bars, 1 mm.

(E) Spatial distribution of individual cells across the sequenced tissue sections.

(F) UMAP embedding showing major cell types identified in control and AC samples.

(legend continued on next page)

an M1 phenotype contributes to a sustained inflammatory milieu.[23,27–30] T cells, largely absent from normal capsules, have been shown to participate in AC pathology, with IL-17A driving both inflammatory and pro-fibrotic responses.[31] In addition, elevated levels of alarmins, including HMGB1, IL-33, and S100A8/A9, correlate with pain severity and may further amplify inflammation, fibrosis, and nerve growth.[32] While these studies have provided important insights, inflammation alone does not fully explain the persistent fibrosis that defines AC.

Fibrosis represents the core pathological process in AC, and fibroblasts are the principal effector cells responsible for extracellular matrix (ECM) production, remodeling, and contraction within the joint capsule. Fibroblasts constitute the most abundant stromal population in capsular tissue. In healthy capsules, type I collagen predominates, whereas AC tissues exhibit excessive deposition of immature and disorganized type III collagen, along with increased expression of fibronectin and tenascin C.[33–36] Transforming growth factor β (TGF-β), a central driver of fibrogenesis, is markedly upregulated in AC and promotes fibroblast proliferation, myofibroblast differentiation, ECM accumulation, and tissue contraction.[37–40] Recent single-cell studies have begun to reveal cellular heterogeneity within the AC joint capsule, including distinct macrophage subsets with pro-resolving or pro-inflammatory functions and their interactions with specific fibroblast populations.[41,42] Activated fibroblasts expressing markers such as CD44, CD55, CD90, VCAM1, and CD248 have been implicated in joint inflammation and matrix dysregulation.[43,44] However, how fibroblast homeostasis is disrupted, how distinct fibroblast states emerge, and which fibroblast populations actively drive fibrotic progression in AC remain largely unresolved.

In this study, we address these knowledge gaps by applying high-resolution spatial transcriptomic profiling to human shoulder joint capsule tissues from patients with AC and non-AC controls. By integrating *in situ* single-cell transcriptomics, computational trajectory inference, and immunofluorescence validation, we systematically map fibroblast heterogeneity, spatial organization, and state transitions within the joint capsule. We identify a disease-enriched fibroblast population characterized by activation of immediate-early gene (IEG) programs and demonstrate its central association with fibrotic remodeling in AC. These findings provide a mechanistic framework linking stress-responsive fibroblast activation to capsular fibrosis and highlight fibroblast state modulation as a potential therapeutic avenue in AC.

RESULTS

Spatial transcriptomics reveals a shift in fibroblast states in AC

Clinical specimens of joint capsules were obtained from intraoperative biopsies during arthroscopic surgery in patients with AC and non-AC controls. Masson's trichrome staining of shoulder joint capsule sections revealed orderly organized ECM fibers in the control groups, whereas ECM fibers in AC specimens exhibited fragmentation and disorganized orientation with remarkably elevated blood vessels (Figure 1A). Quantitative analysis using *CurveAlign* showed that ECM fibers in AC capsules had significantly lower alignment scores and a greater proportion of vascular areas compared to control capsules (Figure 1B). These features represent the clinical characteristics of AC.

To investigate the cellular and molecular mechanisms underlying fibrotic remodeling in AC, we applied CosMx Spatial Molecular Imager (SMI) spatial transcriptomic analysis to profile the cellular microenvironment of adhesive and non-adhesive shoulder joint capsules. This *in situ* hybridization-based approach enables single-cell-resolution spatial mapping of transcriptionally defined cell states, allowing precise localization of disease-associated cell populations and their interactions within the joint capsules (Figure 1C). Sections of three samples from AC and non-AC control groups were histologically examined with hematoxylin and eosin (H&E) staining and selected for downstream processing for spatial transcriptomic imaging (Figure 1D).

After rigorous quality control, a total of 72,865 cells were retained for downstream analysis. The resulting spatial distribution of cells across individual samples is shown in Figure 1E. Following batch integration using *Harmony* and uniform manifold approximation and projection (UMAP) projection, cells were clustered into five major cell types: endothelial cells, fibroblasts, lymphoid cells, myeloid cells, and pericytes (Figure 1F). Distinct transcriptional features and representative marker genes defining each cell type are presented in a heatmap (Figure 1G). Inspection of the UMAP embedding and fibroblast-specific marker expression revealed pronounced intra-population heterogeneity within the fibroblast compartment, indicating the presence of distinct fibroblast subsets (Figures 1F and 1G). However, the overall cellular composition did not differ significantly between AC and non-AC control tissues (Figures 1H and 1I). Thus, rather than a change in fibroblast abundance, AC is characterized by a shift in fibroblast states and subpopulation composition.

Emergence of IEG-activated fibroblasts in AC

Given the pronounced heterogeneity of fibroblasts in AC, we next resolved fibroblast subpopulations at higher resolution. UMAP-based clustering delineated three transcriptionally distinct fibroblast subsets (Figure 2A).

The first subset, FB1, was characterized by high expression of *PTEN* and *RASA4* (Figure 2B). PTEN negatively regulates PI3K/AKT/mTOR signaling, while RASA4 functions as a Ras GTPase-activating protein that attenuates Ras/mitogen-activated protein kinase (MAPK) pathway activity. The coordinated expression of these negative signaling regulators suggests that FB1 represents a homeostatic or quiescent fibroblast population with dampened mitogenic and pro-fibrotic signaling.

(G) Heatmap displaying feature marker genes defining each major cell type.
(H) Relative proportions of major cell types in the control and AC groups.
(I) Quantitative comparison of cell type proportions between control and AC samples (n = 3). Data are presented as mean ± SD. Statistical significance was assessed using unpaired two-tailed Student's t tests. ***$p < 0.001$, ****$p < 0.0001$.

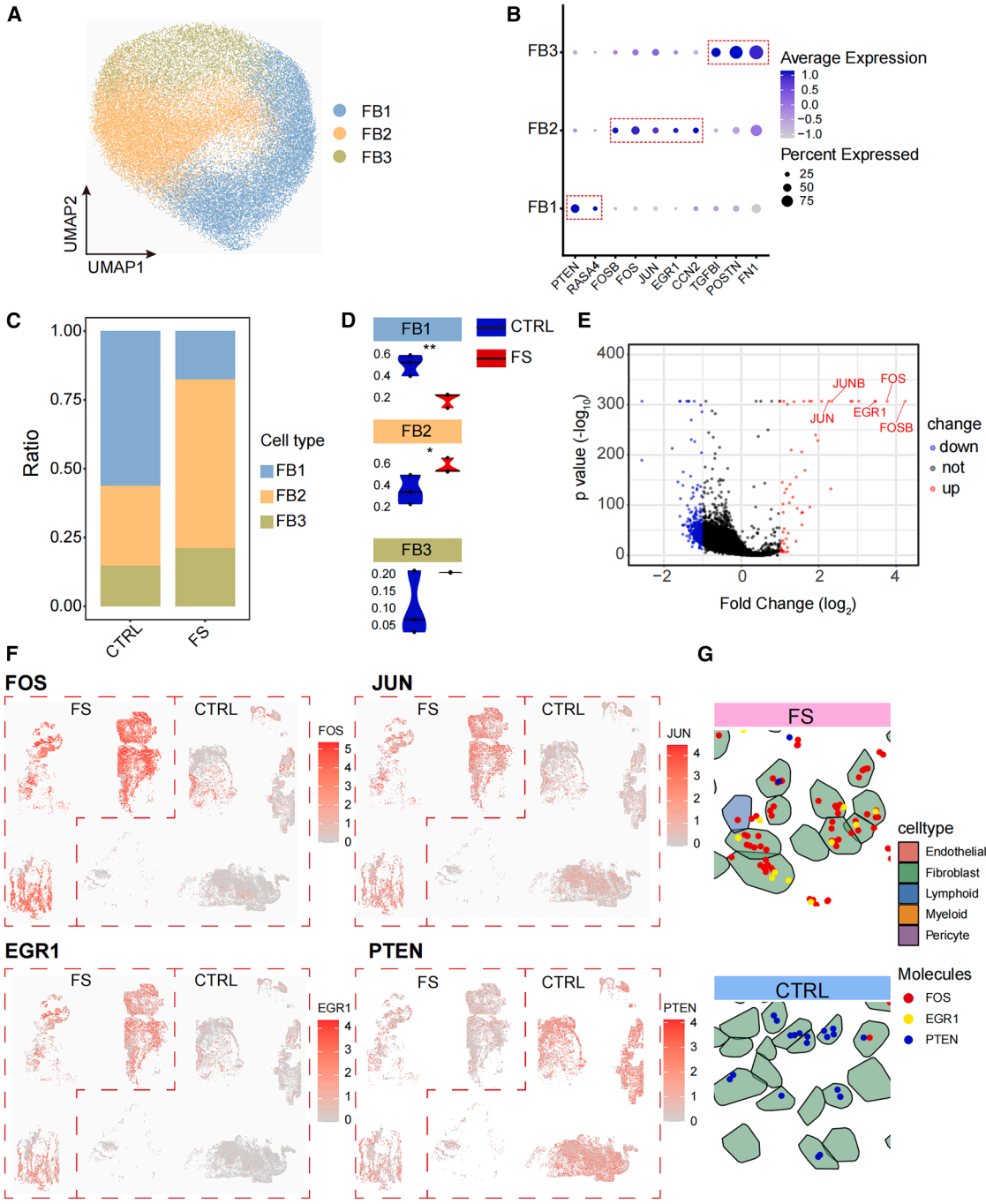

Figure 2. Emergence of IEG-activated fibroblasts in frozen shoulder

(A) UMAP embedding showing the segregation of fibroblasts into distinct transcriptional subpopulations.

(B) Dot plot displaying feature marker gene expression across fibroblast subpopulations.

(C) Relative proportions of fibroblast subpopulations in control and AC samples.

(D) Quantitative comparison of fibroblast subpopulation proportions between control and AC groups (n = 3).

(E) Differentially expressed genes (DEGs) in fibroblasts from AC compared with control samples. IEGs among the top ten upregulated DEGs are indicated.

(F) Spatial mapping of representative FB1- and FB2-associated genes in control and AC joint capsule tissues.

(G) High-resolution spatial visualization at single-cell resolution. Colored cell boundaries denote individual cells, while overlaid dots indicate detected transcript signals. Data are presented as mean ± SD. Statistical significance was assessed using unpaired two-tailed Student's t tests.*$p < 0.05$, **$p < 0.01$.

The second fibroblast subset, FB2, was distinguished by high expression of IEGs, including *FOSB*, *JUN*, and *EGR1*, together with the pro-fibrotic mediator *CCN2* (Figure 2B). FOS and JUN family members form the AP-1 transcription factor complex, a stress- and stimulus-responsive regulator that rapidly integrates extracellular signals to control gene programs associated with cell activation, proliferation, inflammation, and ECM remodeling. EGR1, a canonical immediate-early zinc-finger transcription factor, further supports the rapid-response nature of this subset. In addition, elevated expression of CCN2, which encodes connective tissue growth factor (CTGF), a key mediator of fibrotic remodeling, links this early activation program to downstream pro-fibrotic responses. Based on these transcriptional features, FB2 was defined as an IEG-activated fibroblast subset.

The third fibroblast subset, FB3, exhibited high expression of canonical fibrosis-associated genes, including *TGFBI*, *POSTN*, and *FN1* (Figure 2B). These genes are hallmarks of ECM production and tissue remodeling, indicating a late-stage, matrix-producing fibroblast state. Accordingly, FB3 was classified as a pro-fibrotic, late-activation fibroblast population.

Comparison of fibroblast subset composition between AC and control samples revealed a significant reduction in homeostatic FB1 and marked expansion of IEG-activated FB2 in AC joint capsules (Figures 2C and 2D). Consistent with this shift, differential gene expression analysis of fibroblasts identified 346 genes significantly upregulated and 55 genes down-regulated in AC compared with non-AC samples. Notably, five canonical IEGs, including *FOS*, *FOSB*, *JUN*, *JUNB*, and *EGR1*, ranked among the top ten upregulated transcripts (Figure 2E), highlighting a dominant immediate-early transcriptional program in AC fibroblasts that closely matched the FB2 state.

Spatial mapping further demonstrated preferential expression of FB2-associated IEGs (*FOS*, *JUN*, and *EGR1*) in AC joint capsules, whereas *PTEN*, a defining marker of homeostatic FB1, was predominantly enriched in non-AC controls (Figure 2F). High-resolution spatial visualization at single-cell resolution confirmed distinct cellular localization patterns of these markers. In these images, fibroblasts are delineated in green with clear cell boundaries, and individual transcripts are visualized as colored dots: *FOS* in red, *EGR1* in yellow, and *PTEN* in blue. *FOS* and *EGR1* transcripts were strongly enriched within fibroblasts in AC samples, whereas *PTEN* transcripts were preferentially localized to fibroblasts in control tissues (Figure 2G). These data provide direct *in situ* evidence for disease-specific fibroblast activation states.

Together, these results demonstrate that an IEG-activated fibroblast subset is selectively enriched in AC, while remaining rare in non-AC joint capsules. This population represents a rapidly inducible fibroblast state associated with pathological activation and likely plays a central role in driving fibrotic remodeling in AC.

Trajectory analysis reveals a sequential transition from homeostatic to pro-fibrotic fibroblast states in AC

To further investigate potential transitions among fibroblast states during the progression of AC, we performed Slingshot-based pseudotime analysis to infer transition trajectories across the three identified fibroblast subsets. This analysis revealed a continuous trajectory progressing from FB1 through FB2 to FB3 (Figure 3A), consistent with a transition from homeostatic fibroblasts to IEG-activated fibroblasts and ultimately to pro-fibrotic, matrix-producing fibroblasts.

Comparison of cell density distributions along the inferred pseudotime axis demonstrated that fibroblasts from non-AC control samples were predominantly positioned at early states corresponding to FB1, whereas fibroblasts from AC samples were enriched at a later state associated with the IEG-activated FB2 phenotype (Figure 3B). Based on transcriptomic similarity, we infer that a pre-activation state of joint capsule fibroblasts marked by high expression of IEGs may predispose to the progression of AC.

To explore molecular pathways underlying the transition from homeostatic to IEG-activated fibroblasts, we compared the transcriptomes of FB2 fibroblasts from AC samples and FB1 fibroblasts from the non-AC samples. Gene set enrichment analysis (GSEA)-based Kyoto Encyclopedia of Genes and Genomes (KEGG) pathway enrichment analysis of differentially expressed genes revealed significant activation of the MAPK, IL-17, and TNF signaling pathways (Figure 3C). Consistently, Gene Ontology (GO) functional enrichment analysis highlighted biological processes associated with collagen fibril organization, ECM remodeling, responses to hormonal changes, and TGF-β signaling (Figure 3D). Enrichment plots display the distribution of core pathway genes across the range of $\log_2$ fold changes, with dot size and color indicating the normalized enrichment score (NES) and pathway significance, respectively. Positive NES values (red) reflect pathway activation. These results suggest that early fibroblast activation in AC involves a coordinated program of stress-responsive signaling and matrix remodeling, potentially priming fibroblasts for subsequent fibrotic progression.

In situ validation identifies IEG-activated fibroblasts as a central cellular driver of AC

To validate the fibroblast subsets identified by transcriptomic analyses, we performed immunofluorescence staining on human should joint capsule tissues from patients with AC and non-AC controls. Tissue sections were co-immunolabeled with the pan-fibroblast marker PDGFRα and markers representative of FB1 homeostatic fibroblasts (PTEN) or FB2 IEG-activated fibroblasts (FOS, JUN, EGR1, and CCN2).

In non-AC control samples, $PTEN^+PDGFR\alpha^+$ fibroblasts were readily detected and were predominantly localized to the peripheral regions of the joint capsule, consistent with a quiescent, homeostatic stromal architecture (Figure 4A). In contrast, AC samples showed a marked reduction, approaching nearly complete loss of $PTEN^+$ fibroblasts, indicating a profound depletion of the homeostatic fibroblast population in diseased capsules (Figure 4A).

Conversely, AC joint capsules exhibited a robust accumulation of $FOS^+JUN^+PDGFR\alpha^+$ fibroblasts (Figure 4B). Notably, these AP-1 (Fos/Jun)-expressing fibroblasts were broadly distributed throughout the capsule rather than being confined to peripheral regions, suggesting a widespread stromal activation state. Immunostaining for EGR1 revealed a highly similar spatial pattern, further supporting the expansion of an IEG-activated fibroblast subset in AC (Figure 4C).

Importantly, these IEG-activated fibroblasts displayed elevated expression of CCN2 (CTGF), a key mediator of fibrotic

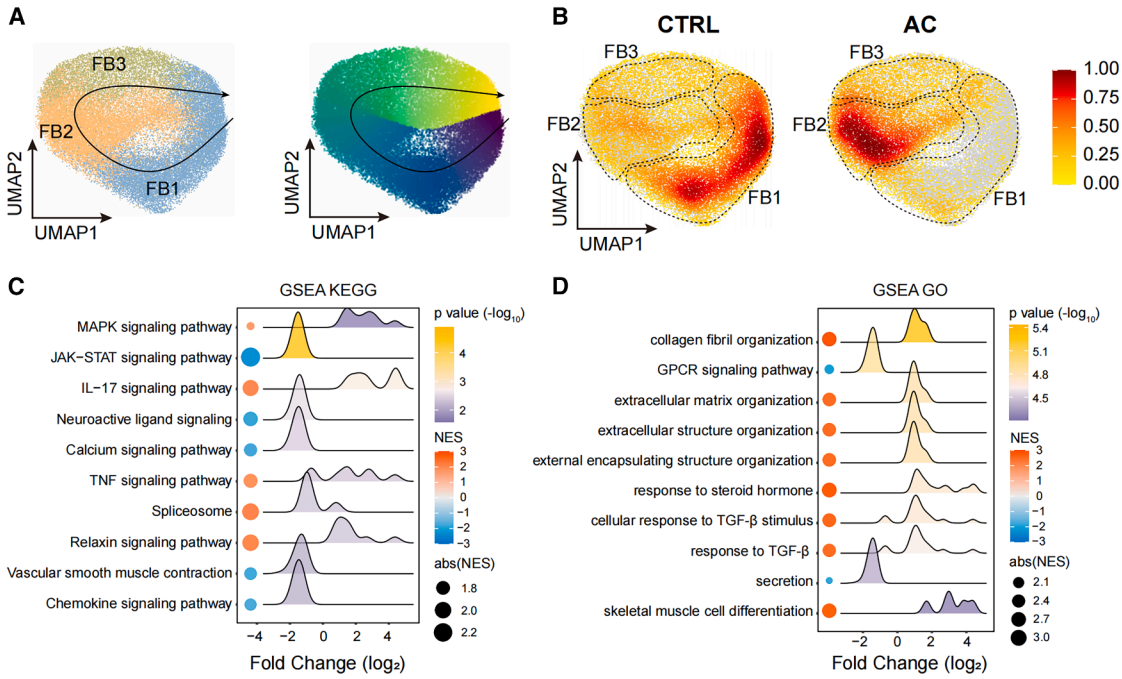

Figure 3. Trajectory analysis reveals a sequential transition from homeostatic to pro-fibrotic fibroblast states in AC

(A) Slingshot-based pseudotime analysis depicting the inferred transition trajectory of fibroblast subpopulations.

(B) Cell density distribution of fibroblasts in control and AC samples. Dashed lines indicate the inferred boundaries between fibroblast subpopulations.

(C) GSEA-based KEGG pathway enrichment analysis of differentially expressed genes (DEGs) comparing FB2 fibroblasts from AC samples with FB1 fibroblasts from non-AC controls.

(D) GSEA-based Gene Ontology (GO) biological process enrichment analysis of the same DEG set. NES, normalized enrichment score.

remodeling, indicating that they represent an early pro-fibrotic fibroblast state rather than terminally differentiated myofibroblasts (Figure 4D). In line with this notion, classic mature myofibroblast markers αSMA and TGF-β1 were expressed at relatively low levels in PDGFRα$^+$ fibroblasts overall, although the proportion of αSMA$^+$ or TGF-β1$^+$ fibroblasts was modestly but significantly increased in AC samples compared with controls (Figures 4E and 4F).

DISCUSSION

Our data reveal a profound reorganization of the fibroblast landscape in AC, characterized by the loss of homeostatic fibroblasts and the emergence of a dominant stress-responsive population. This IEG-activated fibroblast state, defined by strong AP-1 (Fos/Jun) and EGR1 activity together with early pro-fibrotic features such as CCN2 upregulation, is rare in normal joint capsules but becomes spatially widespread in disease. Pseudotime analysis places these cells in a transitional position rather than at a terminal myofibroblast endpoint, suggesting that capsular remodeling in AC is driven by fibroblast plasticity and state switching, rather than by the simple accumulation of fully differentiated fibrotic cells.

Integrating these findings, we propose a model (Figure 5) in which sustained stress exposure is associated with the emergence of an IEG-activated fibroblast state in the joint capsule through stress-responsive signaling programs, plausibly involving MAPK, IL-17, and TNF-associated transcriptional outputs. This framework suggests a potential continuum of fibroblast states, in which these primed fibroblasts may amplify inflammatory and fibrogenic signals and facilitate subsequent engagement of TGF-β-dependent matrix remodeling pathways, thereby contributing to capsular fibrosis. Although this model is inferred from transcriptional state transitions rather than direct lineage tracing, it provides a coherent mechanistic framework linking stress adaptation, fibroblast state switching, and progressive fibrosis in AC.

IEGs such as *FOS*, *JUN*, and *EGR1* are rapidly and transiently induced in response to extracellular stimuli, including mechanical stress, cytokines, growth factors, and neurotransmitters, independently of *de novo* protein synthesis.[45] Activation of these genes represents a conserved cellular program that enables cells to sense environmental perturbations and initiate adaptive responses.[46] In fibroblasts, IEG activation has been increasingly recognized as an early and decisive event preceding fibrotic differentiation. In pulmonary, renal, and cardiac fibrosis, stress-responsive transcription factors, particularly AP-1 components and EGR family members, have been shown to promote fibroblast activation, inflammatory crosstalk, and ECM remodeling.[47–52] Our findings extend this concept to AC, demonstrating that IEG-activated fibroblasts emerge as a distinct and spatially organized population within the joint capsule and are preferentially enriched in disease. While IEG activation represents a general cellular response to stress, our data indicate that this

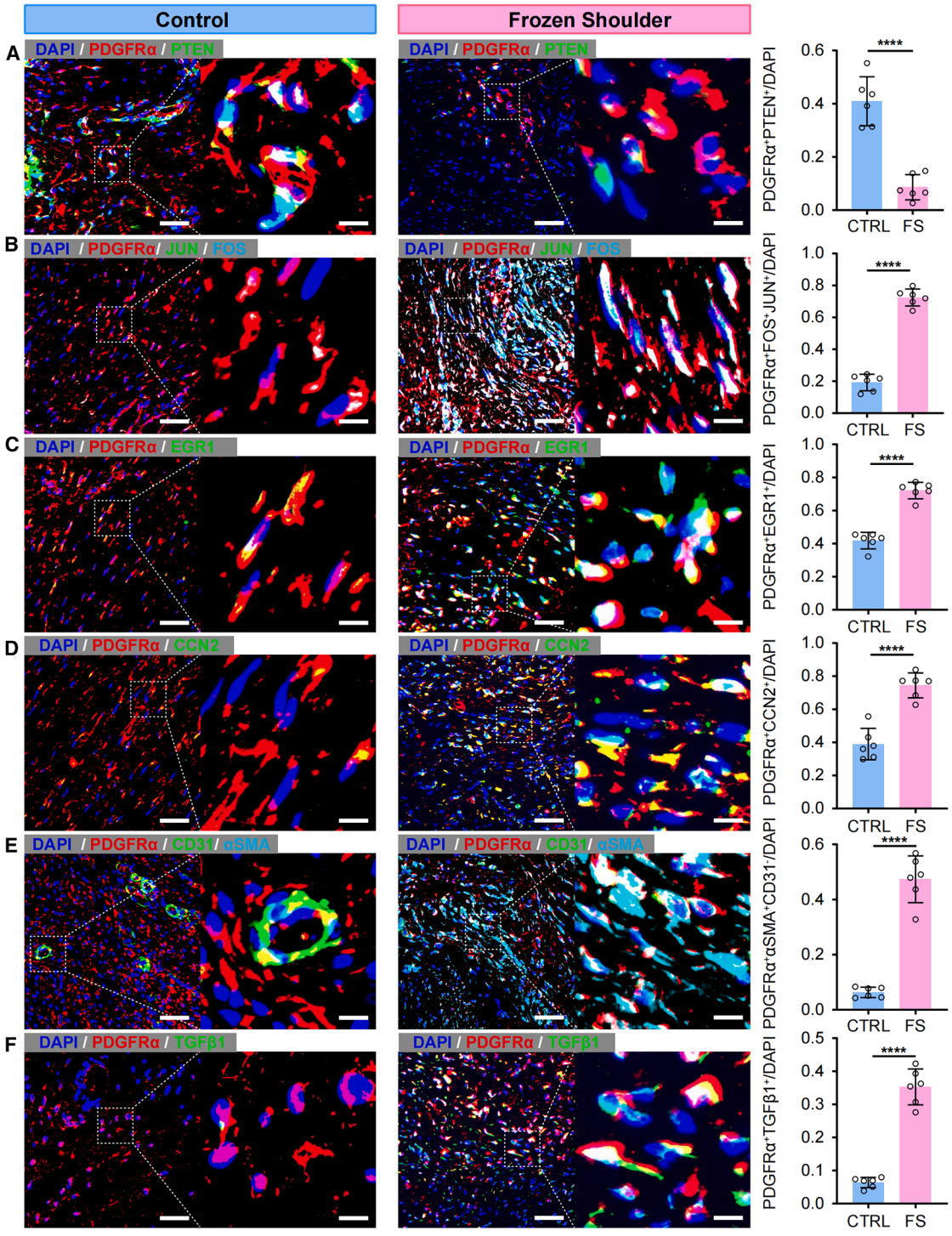

Figure 4. *In situ* validation identifies IEG-activated fibroblasts as a central cellular driver of AC

Representative immunofluorescence staining of joint capsular tissues from the control and AC groups showing pan-fibroblast marker PDGFRα in combination with PTEN (A), JUN and FOS (B), EGR1 (C), CCN2 (D), CD31 and αSMA (E), or TGF-β1 (F), together with quantification of the corresponding positive cell proportions. Scale bars, 50 μm; inset, 10 μm. Data are presented as mean ± SD (n = 6). Statistical significance was determined by unpaired two-tailed Student's t tests. ****$p < 0.0001$.

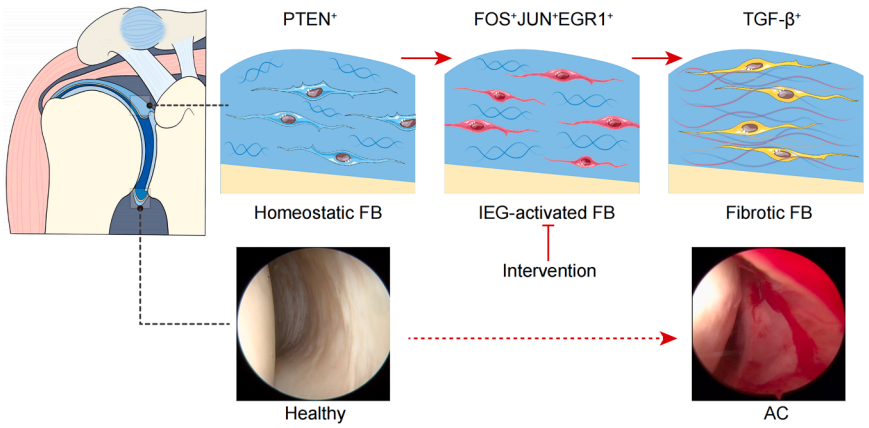

Figure 5. Schematic of the sequential transition of fibroblast subpopulations during AC progression

response is selectively expanded and spatially organized within the fibroblast compartment in frozen shoulder, suggesting a disease-associated amplification of this program rather than a uniform tissue-wide response. The concurrent upregulation of the CTGF-encoding gene *CCN2* further links this early activation program to sustained pro-fibrotic signaling, consistent with the known synergy between CTGF and TGF-β in reinforcing fibrotic responses across tissues.[53]

Notably, much of the existing literature on AC and fibrosis more broadly has focused on terminally differentiated, αSMA$^+$ myofibroblasts and canonical TGF-β signaling.[54–56] While these cells represent key effectors of tissue contraction and matrix deposition, accumulating evidence across multiple organs, including the liver, lung, heart, skin, and kidney, suggests that established myofibroblast states are highly resistant to reversal.[57–61] Our data support a model in which fibroblast activation is not a binary switch but a continuum, with an intermediate IEG-activated state bridging homeostasis and overt fibrosis. In AC, this intermediate state is marked by rapid stress responsiveness, inflammatory signaling, and early matrix remodeling capacity. Importantly, targeting fibroblasts at this early activation stage may provide a broader therapeutic window to halt or reverse disease progression before irreversible capsular fibrosis is established.

In summary, this study reveals a previously unrecognized stress-responsive fibroblast state that bridges inflammation and fibrosis in frozen shoulder. By highlighting IEG-activated fibroblasts as a pivotal intermediate in disease progression, our findings provide new conceptual insight into capsular fibrosis and suggest potential therapeutic strategies aimed at restoring fibroblast homeostasis or interrupting early activation programs to prevent irreversible joint contracture.

Limitations of the study

Several limitations of this study should be acknowledged. First, the cross-sectional analysis of human surgical specimens precludes direct observation of dynamic state transitions. Consequently, the trajectories inferred from spatial transcriptomics and pseudotime analysis will require further validation in longitudinal studies or animal models. Second, although our data highlight the potential involvement of MAPK and TGF-β signaling programs in fibroblast state transitions, functional perturbation studies will be necessary to establish causal relationships. Third, although CosMx SMI spatial transcriptomic imaging has certain advantages in accuracy and localization due to its principle of *in situ* hybridization, the number of RNA molecules it can detect remains inferior to that of PCR-based sequencing technologies. Finally, the upstream niche signals that initiate IEG activation in joint capsule fibroblasts remain to be elucidated. Future studies should also explore reciprocal interactions between fibroblasts and immune cells that may contribute to shaping the fibrotic microenvironment in frozen shoulder. Despite these limitations, our spatially resolved analysis of human capsule tissue provides a framework for understanding fibroblast state heterogeneity and its potential relevance to capsular fibrosis.

RESOURCE AVAILABILITY

Lead contact

Requests for further information and resources should be directed to and will be fulfilled by the lead contact, Chunxi Yang (chunxi_yang@163.com).

Materials availability

This study did not generate new unique reagents.

Data and code availability

The spatial transcriptomics data generated in this study have been deposited in the OMIX with accession number OMIX015211, China National Center for Bioinformation/Beijing Institute of Genomics, Chinese Academy of Sciences (https://ngdc.cncb.ac.cn/omix). This paper does not report original code. Any additional information required to reanalyze the data reported in this paper is available from the lead contact upon request. This paper does not report original code.

ACKNOWLEDGMENTS

C.Y. is supported by the National Natural Science Foundation of China (no. 82372488). D.J. is supported by the National Natural Science Foundation of China (no. 82573954) and the Natural Science Foundation of Shanghai (no. 25ZR1401298).

AUTHOR CONTRIBUTIONS

Conceptualization, C.Y., D.J., and Z.R.; investigation, Z.R., J.L., R.W., W.N., X.Z., and Y.H.; human sample provision, C.Y.; data curation, Z.R., J.L., D.J., and C.Y.; writing – original draft, Z.R. and D.J.; writing – review and editing,

C.Y., D.J., H.L., and Z.R.; funding acquisition, C.Y. and D.J.; supervision, D.J., H.L., and C.Y.; project administration, C.Y. and D.J. All authors reviewed the manuscript.

DECLARATION OF INTERESTS

The authors declare no competing of interests.

STAR★METHODS

Detailed methods are provided in the online version of this paper and include the following:

- KEY RESOURCES TABLE
- EXPERIMENTAL MODEL AND STUDY PARTICIPANT DETAILS
  - Human shoulder joint capsule tissues
- METHOD DETAILS
  - Spatial transcriptomic imaging
  - Bioinformatics analysis of SMI data
  - H&E and Masson's trichrome staining
  - Immunofluorescence staining
- QUANTIFICATION AND STATISTICAL ANALYSIS
  - Image quantification and statistical analysis

SUPPLEMENTAL INFORMATION

Supplementary data related to this article can be found online at https://doi.org/10.1016/j.isci.2026.116183.

Received: March 9, 2026
Revised: April 20, 2026
Accepted: May 6, 2026

REFERENCES

1. Millar, N.L., Meakins, A., Struyf, F., Willmore, E., Campbell, A.L., Kirwan, P.D., Akbar, M., Moore, L., Ronquillo, J.C., Murrell, G.A.C., and Rodeo, S.A. (2022). Frozen shoulder. Nat. Rev. Dis. Primers *8*, 59. https://doi.org/10.1038/s41572-022-00386-2.
2. Walker-Bone, K., Palmer, K.T., Reading, I., Coggon, D., and Cooper, C. (2004). Prevalence and impact of musculoskeletal disorders of the upper limb in the general population. Arthritis Rheum. *51*, 642–651. https://doi.org/10.1002/art.20535.
3. Sarasua, S.M., Floyd, S., Bridges, W.C., and Pill, S.G. (2021). The epidemiology and etiology of adhesive capsulitis in the U.S. Medicare population. BMC Muscoskelet. Disord. *22*, 828. https://doi.org/10.1186/s12891-021-04704-9.
4. Alhashimi, R. (2018). Analytical Observational Study of Frozen Shoulder among Patients with Diabetes Mellitus. Joints *06*, 141–144. https://doi.org/10.1055/s-0038-1676105.
5. Schiefer, M., Teixeira, P.F.S., Fontenelle, C., Carminatti, T., Santos, D.A., Righi, L.D., and Conceição, F.L. (2017). Prevalence of hypothyroidism in patients with frozen shoulder. J. Shoulder Elb. Surg. *26*, 49–55. https://doi.org/10.1016/j.jse.2016.04.026.
6. Wang, J.Y., Liaw, C.K., Huang, C.C., Liou, T.H., Lin, H.W., and Huang, S.W. (2021). Hyperlipidemia Is a Risk Factor of Adhesive Capsulitis: Real-World Evidence Using the Taiwanese National Health Insurance Research Database. Orthop. J. Sports Med. *9*, 2325967120986808. https://doi.org/10.1177/2325967120986808.
7. Li, W., Lu, N., Xu, H., Wang, H., and Huang, J. (2015). Case control study of risk factors for frozen shoulder in China. Int. J. Rheum. Dis. *18*, 508–513. https://doi.org/10.1111/1756-185X.12246.
8. Itoi, E., Arce, G., Bain, G.I., Diercks, R.L., Guttmann, D., Imhoff, A.B., Mazzocca, A.D., Sugaya, H., and Yoo, Y.S. (2016). Shoulder Stiffness: Current Concepts and Concerns. Arthroscopy *32*, 1402–1414. https://doi.org/10.1016/j.arthro.2016.03.024.
9. de la Serna, D., Navarro-Ledesma, S., Alayón, F., López, E., and Pruimboom, L. (2021). A Comprehensive View of Frozen Shoulder: A Mystery Syndrome. Front. Med. *8*, 663703. https://doi.org/10.3389/fmed.2021.663703.
10. Juel, N.G., Brox, J.I., Brunborg, C., Holte, K.B., and Berg, T.J. (2017). Very High Prevalence of Frozen Shoulder in Patients With Type 1 Diabetes of >/=45 Years' Duration: The Dialong Shoulder Study. Arch. Phys. Med. Rehabil. *98*, 1551–1559. https://doi.org/10.1016/j.apmr.2017.01.020.
11. Tanishima, T., and Yoshimasu, N. (1997). Development and prevention of frozen shoulder after acute aneurysm surgery. Surg. Neurol. *48*, 19–22.
12. Kim, D.H., Kim, Y.S., Kim, B.S., Sung, D.H., Song, K.S., and Cho, C.H. (2020). Is frozen shoulder completely resolved at 2 years after the onset of disease? J. Orthop. Sci. *25*, 224–228. https://doi.org/10.1016/j.jos.2019.03.011.
13. Shaffer, B., Tibone, J.E., and Kerlan, R.K. (1992). Frozen shoulder. A long-term follow-up. J. Bone Joint Surg. *74*, 738–746.
14. Hand, C., Clipsham, K., Rees, J.L., and Carr, A.J. (2008). Long-term outcome of frozen shoulder. J. Shoulder Elb. Surg. *17*, 231–236. https://doi.org/10.1016/j.jse.2007.05.009.
15. Rangan, A., Brealey, S.D., Keding, A., Corbacho, B., Northgraves, M., Kottam, L., Goodchild, L., Srikesavan, C., Rex, S., Charalambous, C.P., et al. (2020). Management of adults with primary frozen shoulder in secondary care (UK FROST): a multicentre, pragmatic, three-arm, superiority randomised clinical trial. Lancet *396*, 977–989. https://doi.org/10.1016/S0140-6736(20)31965-6.
16. Le, H.V., Lee, S.J., Nazarian, A., and Rodriguez, E.K. (2017). Adhesive capsulitis of the shoulder: review of pathophysiology and current clinical treatments. Shoulder Elbow *9*, 75–84. https://doi.org/10.1177/1758573216676786.
17. Muthukrishnan, R., Rashid, A.A., and Al-Alkharji, F. (2019). The effectiveness of extracorporeal shockwave therapy for frozen shoulder in patients with diabetes: randomized control trial. J. Phys. Ther. Sci. *31*, 493–497.
18. Poku, D., Hassan, R., Migliorini, F., and Maffulli, N. (2023). Efficacy of hydrodilatation in frozen shoulder: a systematic review and meta-analysis. Br. Med. Bull. *147*, 121–147. https://doi.org/10.1093/bmb/ldad018.
19. Challoumas, D., Biddle, M., McLean, M., and Millar, N.L. (2020). Comparison of Treatments for Frozen Shoulder: A Systematic Review and Meta-analysis. JAMA Netw. Open *3*, e2029581. https://doi.org/10.1001/jamanetworkopen.2020.29581.
20. Zhang, R., Wang, Z., Liu, R., Zhang, N., Guo, J., and Huang, Y. (2022). Extracorporeal Shockwave Therapy as an Adjunctive Therapy for Frozen Shoulder: A Systematic Review and Meta-analysis. Orthop. J. Sports Med. *10*, 23259671211062222. https://doi.org/10.1177/23259671211062222.
21. Kirker, K., O'Connell, M., Bradley, L., Torres-Panchame, R.E., and Masaracchio, M. (2023). Manual therapy and exercise for adhesive capsulitis: a systematic review with meta-analysis. J. Man. Manip. Ther. *31*, 311–327. https://doi.org/10.1080/10669817.2023.2180702.
22. Xu, Y., Bonar, F., and Murrell, G.A.C. (2012). Enhanced expression of neuronal proteins in idiopathic frozen shoulder. J. Shoulder Elb. Surg. *21*, 1391–1397. https://doi.org/10.1016/j.jse.2011.08.046.
23. Lho, Y.M., Ha, E., Cho, C.H., Song, K.S., Min, B.W., Bae, K.C., Lee, K.J., Hwang, I., and Park, H.B. (2013). Inflammatory cytokines are overexpressed in the subacromial bursa of frozen shoulder. J. Shoulder Elb. Surg. *22*, 666–672. https://doi.org/10.1016/j.jse.2012.06.014.
24. Ryan, V., Brown, H., Minns Lowe, C.J., and Lewis, J.S. (2016). The pathophysiology associated with primary (idiopathic) frozen shoulder: A systematic review. BMC Muscoskelet. Disord. *17*, 340. https://doi.org/10.1186/s12891-016-1190-9.

25. Hand, G.C.R., Athanasou, N.A., Matthews, T., and Carr, A.J. (2007). The pathology of frozen shoulder. J Bone Joint Surg Br *89-B*, 928–932. https://doi.org/10.1302/0301-620X.89B7.19097.

26. Dakin, S.G., Rangan, A., Martinez, F., Brealey, S., Northgraves, M., Kottam, L., Cooper, C., Buckley, C.D., and Carr, A.J. (2019). Tissue inflammation signatures point towards resolution in adhesive capsulitis. Rheumatology *58*, 1109–1111. https://doi.org/10.1093/rheumatology/kez007.

27. Damerau, A., Rosenow, E., Alkhoury, D., Buttgereit, F., and Gaber, T. (2024). Fibrotic pathways and fibroblast-like synoviocyte phenotypes in osteoarthritis. Front. Immunol. *15*, 1385006. https://doi.org/10.3389/fimmu.2024.1385006.

28. Mattyasovszky, S.G., Mausbach, S., Ritz, U., Langendorf, E., Wollstädter, J., Baranowski, A., Drees, P., Rommens, P.M., and Hofmann, A. (2017). Influence of the anti-inflammatory cytokine interleukin-4 on human joint capsule myofibroblasts. J. Orthop. Res. *35*, 1290–1298. https://doi.org/10.1002/jor.23386.

29. Kaneguchi, A., and Ozawa, J. (2022). Inflammation and Fibrosis Induced by Joint Remobilization, and Relevance to Progression of Arthrogenic Joint Contracture: A Narrative Review. Physiol. Res. *71*, 447–455. https://doi.org/10.33549/physiolres.934876.

30. Kabbabe, B., Ramkumar, S., and Richardson, M. (2010). Cytogenetic analysis of the pathology of frozen shoulder. Int. J. Shoulder Surg. *4*, 75–78. https://doi.org/10.4103/0973-6042.76966.

31. Akbar, M., Crowe, L.A.N., McLean, M., Garcia-Melchor, E., MacDonald, L., Carter, K., Fazzi, U.G., Martin, D., Arthur, A., Reilly, J.H., et al. (2021). Translational targeting of inflammation and fibrosis in frozen shoulder: Molecular dissection of the T cell/IL-17A axis. Proc. Natl. Acad. Sci. USA *118*, e2102715118. https://doi.org/10.1073/pnas.2102715118.

32. Cher, J.Z.B., Akbar, M., Kitson, S., Crowe, L.A.N., Garcia-Melchor, E., Hannah, S.C., McLean, M., Fazzi, U.G., Kerr, S.C., Murrell, G.A.C., and Millar, N.L. (2018). Alarmins in Frozen Shoulder: A Molecular Association Between Inflammation and Pain. Am. J. Sports Med. *46*, 671–678. https://doi.org/10.1177/0363546517741127.

33. Liu, Y.-L., Ao, Y.-F., Cui, G.-Q., and Zhu, J.-X. (2011). Changes of histology and capsular collagen in a rat shoulder immobilization model. Chin. Med. J. *124*, 3939–3944.

34. Marker, L., Schjerling, P., Mackey, A.L., Hansen, T., Jakobsen, J., Kjær, M., and Krogsgaard, M.R. (2021). Collagens in primary frozen shoulder: expression of collagen mRNA isoforms in the different phases of the disease. Rheumatology *60*, 3879–3887. https://doi.org/10.1093/rheumatology/keaa802.

35. Rodeo, S.A., Hannafin, J.A., Tom, J., Warren, R.F., and Wickiewicz, T.L. (1997). Immunolocalization of cytokines and their receptors in adhesive capsulitis of the shoulder. J. Orthop. Res. *15*, 427–436. https://doi.org/10.1002/jor.1100150316.

36. Cho, C.H., Song, K.S., Kim, B.S., Kim, D.H., and Lho, Y.M. (2018). Biological Aspect of Pathophysiology for Frozen Shoulder. Biomed Res. Int. *2018*, 1–8. https://doi.org/10.1155/2018/7274517.

37. Frangogiannis, N.G. (2020). Transforming growth factor-beta in tissue fibrosis. J. Exp. Med. *217*, e20190103. https://doi.org/10.1084/jem.20190103.

38. Liu, Z., Pei, Y., Zeng, H., Yang, Y., Que, M., Xiao, Y., Wang, J., and Weng, X. (2021). Recombinant TSG-6 protein inhibits the growth of capsule fibroblasts in frozen shoulder via suppressing the TGF-beta/Smad2 signal pathway. J. Orthop. Surg. Res. *16*, 564. https://doi.org/10.1186/s13018-021-02705-x.

39. Lubis, A.M.T., and Lubis, V.K. (2013). Matrix metalloproteinase, tissue inhibitor of metalloproteinase and transforming growth factor-beta 1 in frozen shoulder, and their changes as response to intensive stretching and supervised neglect exercise. J. Orthop. Sci. *18*, 519–527. https://doi.org/10.1007/s00776-013-0387-0.

40. Zhang, Y., Liu, Z., Wang, K., Lu, S., Fan, S., Xu, L., and Cai, B. (2021). Macrophage migration inhibitory factor regulates joint capsule fibrosis by promoting TGF-beta1 production in fibroblasts. Int. J. Biol. Sci. *17*, 1837–1850. https://doi.org/10.7150/ijbs.57025.

41. Alivernini, S., MacDonald, L., Elmesmari, A., Finlay, S., Tolusso, B., Gigante, M.R., Petricca, L., Di Mario, C., Bui, L., Perniola, S., et al. (2020). Distinct synovial tissue macrophage subsets regulate inflammation and remission in rheumatoid arthritis. Nat. Med. *26*, 1295–1306. https://doi.org/10.1038/s41591-020-0939-8.

42. Ng, M.T.H., Borst, R., Gacaferi, H., Davidson, S., Ackerman, J.E., Johnson, P.A., Machado, C.C., Reekie, I., Attar, M., Windell, D., et al. (2024). A single cell atlas of frozen shoulder capsule identifies features associated with inflammatory fibrosis resolution. Nat. Commun. *15*, 1394. https://doi.org/10.1038/s41467-024-45341-9.

43. Millar, N.L., Silbernagel, K.G., Thorborg, K., Kirwan, P.D., Galatz, L.M., Abrams, G.D., Murrell, G.A.C., McInnes, I.B., and Rodeo, S.A. (2021). Tendinopathy. Nat. Rev. Dis. Primers *7*, 1. https://doi.org/10.1038/s41572-020-00234-1.

44. Dakin, S.G., Buckley, C.D., Al-Mossawi, M.H., Hedley, R., Martinez, F.O., Wheway, K., Watkins, B., and Carr, A.J. (2017). Persistent stromal fibroblast activation is present in chronic tendinopathy. Arthritis Res. Ther. *19*, 16. https://doi.org/10.1186/s13075-016-1218-4.

45. Abraham, W.C., Dragunow, M., and Tate, W.P. (1991). The role of immediate early genes in the stabilization of long-term potentiation. Mol. Neurobiol. *5*, 297–314.

46. Healy, S., Khan, P., and Davie, J.R. (2013). Immediate early response genes and cell transformation. Pharmacol. Ther. *137*, 64–77. https://doi.org/10.1016/j.pharmthera.2012.09.001.

47. Ucero, A.C., Bakiri, L., Roediger, B., Suzuki, M., Jimenez, M., Mandal, P., Braghetta, P., Bonaldo, P., Paz-Ares, L., Fustero-Torre, C., et al. (2019). Fra-2-expressing macrophages promote lung fibrosis in mice. J. Clin. Investig. *129*, 3293–3309. https://doi.org/10.1172/JCI125366.

48. Wang, Q., Liu, J., Hu, Y., Pan, T., Xu, Y., Yu, J., Xiong, W., Zhou, Q., and Wang, Y. (2021). Local administration of liposomal-based Srpx2 gene therapy reverses pulmonary fibrosis by blockading fibroblast-to-myofibroblast transition. Theranostics *11*, 7110–7125. https://doi.org/10.7150/thno.61085.

49. Eferl, R., Hasselblatt, P., Rath, M., Popper, H., Zenz, R., Komnenovic, V., Idarraga, M.-H., Kenner, L., and Wagner, E.F. (2008). Development of Pulmonary Fibrosis through a Pathway Involving the Transcription Factor Fra-2/AP-1. Proc. Natl. Acad. Sci. USA *105*, 10525–10530.

50. Yi, H., Jiang, Y., Li, W., Shen, L., Zhang, W., Li, S., Xu, Y., and Li, F. (2025). Scutellarin prevents obesity-induced renal fibrosis via reduced activation of AP-1. J. Transl. Med. *23*, 611. https://doi.org/10.1186/s12967-025-06616-x.

51. Khachigian, L.M. (2024). Early growth response-1, a dynamic conduit in cardiovascular disease. Front. Cardiovasc. Med. *11*, 1487668. https://doi.org/10.3389/fcvm.2024.1487668.

52. Lu, G., Ge, Z., Chen, X., Ma, Y., Yuan, A., Xie, Y., and Pu, J. (2023). BMP6 knockdown enhances cardiac fibrosis in a mouse myocardial infarction model by upregulating AP-1/CEMIP expression. Clin. Transl. Med. *13*, e1296. https://doi.org/10.1002/ctm2.1296.

53. Li, Z., Jiang, J., Cai, K., Qiao, Y., Zhang, X., Wang, L., Kang, Y., Wu, X., Zhao, B., Wang, X., et al. (2025). CCN2 mediates fibroblast-macrophage interaction in knee arthrofibrosis based on single-cell RNA-seq analysis. Bone Res. *13*, 26. https://doi.org/10.1038/s41413-025-00400-9.

54. Jump, C.M., Duke, K., Malik, R.A., and Charalambous, C.P. (2021). Frozen Shoulder: A Systematic Review of Cellular, Molecular, and Metabolic Findings. JBJS Rev. *9*, e19.00153. https://doi.org/10.2106/JBJS.RVW.19.00153.

55. Kanbe, K., Inoue, K., Inoue, Y., and Chen, Q. (2009). Inducement of mitogen-activated protein kinases in frozen shoulders. J. Orthop. Sci. *14*, 56–61. https://doi.org/10.1007/s00776-008-1295-6.

56. Xue, M., Gong, S., Dai, J., Chen, G., and Hu, J. (2016). The Treatment of Fibrosis of Joint Synovium and Frozen Shoulder by Smad4 Gene Silencing

in Rats. PLoS One *11*, e0158093. https://doi.org/10.1371/journal.pone.0158093.

57. Younesi, F.S., Miller, A.E., Barker, T.H., Rossi, F.M.V., and Hinz, B. (2024). Fibroblast and myofibroblast activation in normal tissue repair and fibrosis. Nat. Rev. Mol. Cell Biol. *25*, 617–638. https://doi.org/10.1038/s41580-024-00716-0.

58. Ramachandran, P., Dobie, R., Wilson-Kanamori, J.R., Dora, E.F., Henderson, B.E.P., Luu, N.T., Portman, J.R., Matchett, K.P., Brice, M., Marwick, J.A., et al. (2019). Resolving the fibrotic niche of human liver cirrhosis at single-cell level. Nature *575*, 512–518. https://doi.org/10.1038/s41586-019-1631-3.

59. Reyfman, P.A., Walter, J.M., Joshi, N., Anekalla, K.R., McQuattie-Pimentel, A.C., Chiu, S., Fernandez, R., Akbarpour, M., Chen, C.I., Ren, Z., et al. (2019). Single-Cell Transcriptomic Analysis of Human Lung Provides Insights into the Pathobiology of Pulmonary Fibrosis. Am. J. Respir. Crit. Care Med. *199*, 1517–1536. https://doi.org/10.1164/rccm.201712-2410OC.

60. Liu, M., López de Juan Abad, B., and Cheng, K. (2021). Cardiac fibrosis: Myofibroblast-mediated pathological regulation and drug delivery strategies. Adv. Drug Deliv. Rev. *173*, 504–519. https://doi.org/10.1016/j.addr.2021.03.021.

61. Chen, J., Tang, Y., Zhong, Y., Wei, B., Huang, X.R., Tang, P.M.K., Xu, A., and Lan, H.Y. (2022). P2Y12 inhibitor clopidogrel inhibits renal fibrosis by blocking macrophage-to-myofibroblast transition. Mol. Ther. *30*, 3017–3033. https://doi.org/10.1016/j.ymthe.2022.06.019.

62. Bredfeldt, J.S., Liu, Y., Conklin, M.W., Keely, P.J., Mackie, T.R., and Eliceiri, K.W. (2014). Automated quantification of aligned collagen for human breast carcinoma prognosis. J. Pathol. Inform. *5*, 28. https://doi.org/10.4103/2153-3539.139707.

63. Bankhead, P., Loughrey, M.B., Fernández, J.A., Dombrowski, Y., McArt, D.G., Dunne, P.D., McQuaid, S., Gray, R.T., Murray, L.J., Coleman, H.G., et al. (2017). QuPath: Open source software for digital pathology image analysis. Sci. Rep. *7*, 16878. https://doi.org/10.1038/s41598-017-17204-5.

64. Hannafin, J.A., and Chiaia, T.A. (2000). Adhesive capsulitis. A treatment approach. Clin. Orthop. Relat. Res. *372*, 95–109.

STAR★METHODS

KEY RESOURCES TABLE

REAGENT or RESOURCE	SOURCE	IDENTIFIER
Antibodies		
TGF-β1 antibody clone EPR21143	Abcam	Cat#ab215715
c-Jun antibody clone G-4	Santa Cruz	Cat#sc-74543
c-Fos antibody clone 9F6	Cell Signaling	Cat#2250
CD31 antibody	Abcam	Cat#ab28364
Human PDGFRα antibody	R&D	Cat#AF-307-NA
CTGF (CCN2) antibody clone 6B13	Santa Cruz	Cat#sc-101586
PTEN antibody clone 138G6	Cell Signaling	Cat#9559
aSMA antibody clone 1A4	Cell Signaling	Cat#48938
Chemicals, peptides, and recombinant proteins		
pH 9.0 Tris/EDTA buffer	Beyotime	Cat#P0084
donkey serum	MeilunBio	Cat#MB4516-1
Triton X-100	Servicebio	Cat#G3068
antifade mounting media containing DAPI	SouthernBiotech	Cat#0100-20
Critical commercial assays		
HE Stain Kit	Solarbio	Cat#G1121
Masson's trichrome Stain Kit	Solarbio	Cat#G1346
Deposited data		
spatial transcriptomics data	this paper	https://ngdc.cncb.ac.cn/omix accession number OMIX015211
Software and algorithms		
RStudio	RStudio, Inc	RRID: SCR_000432
GraphPad Prism 8	GraphPad software	RRID: SCR_002798
FIJI	NIH	RRID:SCR_002285
CurveAlign (V5.0)	Bredfeldt JS et al.[62]	https://loci.wisc.edu/curvealign/
Qupath (v0.6.0)	Bankhead P et al.[63]	RRID: SCR_018257

EXPERIMENTAL MODEL AND STUDY PARTICIPANT DETAILS

Human shoulder joint capsule tissues

The use of human shoulder joint capsule tissues in this study was approved by the Institutional Review Boards of Shanghai General Hospital (Approval No. YLK[2025]514) and Renji Hospital (Approval No. KY2021-204-B), Shanghai Jiao Tong University School of Medicine. Written informed consent was obtained from all patients in accordance with the Declaration of Helsinki.

Human shoulder capsular tissue samples were obtained during arthroscopic shoulder surgery. Patients were enrolled based on a confirmed diagnosis of adhesive capsulitis (AC) or non-AC controls, determined by clinical symptoms, physical examination of shoulder range of motion, and radiographic evaluation including X-ray and magnetic resonance imaging (MRI). Eligible participants were adults aged 25–80 years of either sex who required arthroscopic surgery for rotator cuff tear, with or without concomitant shoulder stiffness.[64] Patients in the AC group presented with clinically significant shoulder stiffness, whereas control patients exhibited preserved shoulder mobility.

Exclusion criteria included a history of previous surgery on the affected shoulder, radiographic evidence of shoulder fracture, systemic or degenerative inflammatory joint diseases (such as rheumatoid arthritis or osteoarthritis), and receipt of intra-articular corticosteroid injection within one month prior to surgery.

Shoulder capsule samples from seven patients with AC and nine non-AC control patients were included for downstream analyses. Basic demographic and clinical information, including age, sex, and disease stage (for AC patients), as well as sample allocation for specific experiments, are summarized in Table S1. No personally identifiable information was collected or disclosed.

METHOD DETAILS

Spatial transcriptomic imaging

Sample preparation for CosMx SMI

Spatial molecular profiling was performed using the NanoString CosMx Spatial Molecular Imager (SMI) RNA assay according to the manufacturer's manual (MAN-10184), using formalin-fixed paraffin-embedded (FFPE) tissue sections. The FFPE sections were retrieved in 1× Target Retrieval Solution at 100°C for 8 min, followed by digestion with 3 μg/mL Proteinase K in a hybridization oven at 40°C for 15 min. Sections were then incubated with fiducial markers (0.0005% in 2× Saline Sodium Citrate with Tween 20) for 5 min at room temperature in the dark. To visualize cell morphology and guide field of view (FOV) selection, sections were stained with DAPI and a panel of morphology markers, including CD298/B2M, pan-cytokeratin (PanCK), and CD45.

CosMx SMI instrument processing

Prepared slides were loaded onto the NanoString CosMx SMI instrument for imaging and transcription detection. A total of 386 FOVs were selected across the tissue sections, guided by H&E staining to ensure representative regional coverage. Probe hybridization was performed according to the manufacturer's protocol, followed by removal of unbound probes. An imaging buffer was applied prior to image acquisition. Fluorophores linked to reporter probes via photocleavable linkers were sequentially released by UV illumination and washed with strip wash buffer. Fluorescent barcodes were imaged by the CosMx imager, and decoded by probe identity to generate *in situ* transcription detection data at single-molecule resolution.

Image processing and cell segmentation

Raw image processing and feature extraction were performed using an in-house CosMx SMI data processing pipeline which includes registration, feature detection, and localization. z stack images of nuclear ($DAPI^+$) and surface staining were used to define cell boundaries. Cell segmentation was performed using *Cellpose*, a machine learning-based algorithm, to accurately assign transcripts to individual cells and subcellular compartments. Single-cell transcriptomic profiles were generated by aggregating transcript counts assigned to each segmented cell.

Data processing and spatial analysis

Downstream data analysis was performed using Seurat (v5.0.3), scanpy (v1.9.8) and Giotto (v4.0.5). Quality control was conducted following Nanostring's official guidelines. Cells were excluded if the proportion of negative probe counts exceeded 10%. Among the remaining cells, only those with ≥50 total transcript counts, ≥20 detected genes, and a minimal cell area of 50 μm^2 were retained for further analysis.

Dimensionality reduction and graph-based clustering were performed in Scanpy, using the Leiden algorithm. The processed data were then imported into the R for further analysis. Processed data were subsequently imported into R for downstream analyses. Cell type annotation was carried out using InsituType (NanoString) with appropriate reference datasets. Differentially expressed genes for each cluster were identified using the *FindMarkers* function. Spatially co-expressed gene modules were identified using the *InsituCor* R package. For neighborhood analysis, in-house scripts were applied to divide cells into spatial regions (niches). A spatial Delaunay network was constructed based on cell centroid distances using *createSpatialDelaunayNetwork*, followed by *cellProximityEnrichment* to assess spatial enrichment or depletion between pairs of cell types. The spatial transcriptomics data generated in this study have been deposited in the OMIX with accession number OMIX015211, China National Center for Bioinformation/Beijing Institute of Genomics, Chinese Academy of Sciences (https://ngdc.cncb.ac.cn/omix).

Bioinformatics analysis of SMI data

Downstream bioinformatic analyses of spatially resolved single-cell transcriptomic data were performed using Seurat (v5.0.3) in R. Initial quality control involved filtering cells based on the following criteria: a minimum of 200 counts and a minimum of 200 genes detected per cell. A total of 72,865 cells passed these thresholds and were retained for subsequent analysis. Data integration across samples was conducted using Harmony (v1.2.4) to correct for batch effects. This was followed by cell clustering and subpopulation analysis. Pseudotime trajectory analysis was performed using Slingshot (v2.14.0). For functional annotation, KEGG pathway enrichment analysis and Gene Ontology (GO) enrichment analysis were performed utilizing the KEGG and GO databases, respectively. Gene Set Enrichment Analysis (GSEA) was conducted using the GSEABase (1.68.0) package to achieve enrichment of pathways and functions.

H&E and Masson's trichrome staining

FFPE sections of human shoulder capsule tissue were prepared and stained for histological evaluation. Hematoxylin and Eosin (H&E) staining was performed using a commercial staining kit (Solarbio, G1121) according to the manufacturer's protocol. Masson's trichrome staining was conducted using a commercial kit (Solarbio, G1346) to visualize collagen deposition and tissue fibrosis. Briefly, sections were deparaffinized, rehydrated, and then processed sequentially with the respective staining solutions as specified by the kits. After staining, sections were dehydrated, cleared, and mounted with neutral balsam for microscopic examination.

Immunofluorescence staining

FFPE sections of human shoulder capsular tissues were subjected to immunofluorescence staining according to the following protocol. Sections were deparaffinized and rehydrated through a graded ethanol series. Antigen retrieval was performed by incubating

the sections in pH 9.0 Tris/EDTA buffer (Beyotime, P0084) at 100°C for 20 min using a water bath, followed by cooling to room temperature. Sections were then blocked and permeabilized with 5% donkey serum (MeilunBio, MB4516-1) containing 0.3% Triton X-100 (Servicebio, G3068) for 1 h at room temperature. After washing three times with PBS buffer for 5 min each, the sections were incubated with the corresponding primary antibody at 4°C overnight. Following another three washes with PBS (5 min each), the sections were incubated with the fluorophore-conjugated secondary antibodies. Finally, the sections were mounted with antifade mounting media containing DAPI (SouthernBiotech, 0100–20) and imaged under a fluorescence microscope (Zeiss, Axio Imager Z2).

The following primary antibodies were used: PDGFRα (R&D, AF-307-NA polyclonal); TGF-β1 (Abcam, ab215715, clone EPR21143); c-Jun (Santa Cruz, sc-74543, clone G-4); c-Fos (Cell Signaling, 2250, clone 9F6); CD31 (Abcam, ab28364, polyclonal); CTGF (CCN2) (Santa Cruz, sc-101586, clone 6B13); PTEN (Cell Signaling, 9559, clone 138G6); αSMA (Cell Signaling, 48938, clone 1A4).

QUANTIFICATION AND STATISTICAL ANALYSIS

Image quantification and statistical analysis

For quantitative analysis of fiber alignment in Masson's trichrome-stained images, we employed CurveAlign (V5.0)[63] and FIJI. Ten regions were selected from each of the control and adhesive capsulitis groups for quantification, the data were presented as mean ± SD and statistically compared using unpaired two-tailed Student's *t* test. Quantitative analysis of immunofluorescence was performed using Qupath (v0.6.0)[64]. Following cell segmentation, the number of positive cells was counted. Six regions from each of the control and adhesive capsulitis of the shoulder groups were assessed, the data were presented as mean ± SD and analyzed with unpaired two-tailed Student's *t*-tests. Statistical graphs were generated using GraphPad Prism 8. Statistical significance is denoted by asterisks, according to the following convention: not significant (ns) for $p \geq 0.05$; * for $p < 0.05$; ** for $p < 0.01$; *** for $p < 0.001$; **** for $p < 0.0001$. Statistical information relative to the figures was provided in Table S2.